Journal of Applied Physics

RESEARCH ARTICLE | OCTOBER 11 2016

Resonant frequencies of cantilevered sheets under various clamping configurations immersed in fluid

Naijian Shen ; Debadi Chakraborty ; John E. Sader

J. Appl. Phys. 120, 144504 (2016)
https://doi.org/10.1063/1.4964428

Resonant frequencies of cantilevered sheets under various clamping configurations immersed in fluid

Naijian Shen, Debadi Chakraborty, and John E. Sader[a)]
School of Mathematics and Statistics, The University of Melbourne, Victoria 3010, Australia

(Received 11 July 2016; accepted 25 September 2016; published online 11 October 2016)

Immersion of an elastic cantilevered sheet in a fluid can strongly affect its dynamic response. While significant effort has been expended in studying slender cantilevered sheets, the behavior of wide sheets has received far less attention. Here we study the clamping configuration's effect on the vibrational dynamics of wide cantilever sheets of macroscopic size, which naturally generate inviscid flows. Three practically relevant clamping configurations are investigated: clamping into (i) a thin and rigid horizontal plate, (ii) a rigid vertical wall, and (iii) a rigid line. These are found to produce different resonant frequencies, as expected from the nonlocal flows generated by these cantilevers. The resulting formulas are joined to an existing expression for slender cantilevers, leading to a universal formula valid for all aspect ratios (cantilever length/width) and mode numbers; accuracy is verified using finite element analysis. This study is expected to be of practical value in a host of engineering applications, such as those that utilize fluid-structure interactions for energy harvesting and aerodynamic design. *Published by AIP Publishing.*
[http://dx.doi.org/10.1063/1.4964428]

I. INTRODUCTION

Knowledge of the dynamic response of cantilevered structures immersed in fluid has been used in a broad range of applications. These include the development of nanoscale cantilevers for environmental sensing,[1] engineering design of naval vessels,[2–4] imaging and force spectroscopy with atomic force microscopy (AFM),[5–9] microfluidic sensing,[10] and energy harvesting in high Reynolds number flows.[11–17]

While viscosity of the surrounding fluid typically exerts a strong effect on vibrating micro and nanoscale structures,[18] its effect diminishes with increasing device size. For structures of macroscopic size, i.e., of order of meters, viscosity has a negligible influence, and modeling these flows using an inviscid approximation provides a highly accurate framework. Indeed, significant effort has been expended in studying the vibration of elastic structures with this inviscid flow model, leading to a comprehensive understanding of their dynamics and the combined effects of structural and radiation damping, e.g., see Refs. 3, 4, and 19–23. In this article, we focus on the dynamic response of such large scale cantilevers immersed in fluid.

Many analytical and numerical studies have been developed to model the fluid-structure interaction of macroscopic slender cantilevers, i.e., whose aspect ratio (cantilever length/width) greatly exceeds unity. Chu[19] presented an early and widely used study of this problem, deriving a simple formula for the resonant frequencies that exhibits excellent agreement with measurements.[3] Crighton[21] developed a more comprehensive treatment of slender elastic rods in the small and large acoustic wavelength limit, providing strong insight into the physics of their damping mechanisms. Strikingly, he found that intrinsic material damping of cylindrical cantilevers can be comparable with radiation damping due to the generation and propagation of sound waves. In a more recent development, Elmer and Dreier[24] presented a rigorous model for the resonant frequencies in fluid that accounts for the three-dimensional flows generated by long and slender cantilevers vibrating in their higher order flexural modes. This was extended to torsional modes of vibration by van Eysden and Sader,[25] who also presented analytical formulas for both flexural and torsional modes. Importantly, such inviscid analyses also apply to small-scale cantilever devices when operated in their higher-order modes. Flow around a cantilever in these cases is predominantly inviscid due to the thin viscous penetration depths generated at high oscillation frequency.[26]

To account for the effect of finite aspect ratio (length/width), correction factors to the classical resonant frequency formula of Chu[19] have been developed. Pabst[2] proposed an empirical correction (based on measurements) that gives the resonant frequencies of cantilevered sheets with aspect ratios greater than unity. Lindholm[3] extended this empirical approach and provided a formula that admits aspect ratios less than one. In contrast to these studies, which are founded on the slender result of Chu,[19] Atkinson and de Lara[27] theoretically and rigorously studied the opposite limit of zero aspect ratio, i.e., a sheet that is infinitely wide relative to its length. The flow generated by such a 2D cantilever is intrinsically nonlocal with respect to position, i.e., the fluid pressure at any position on the cantilever depends on the complete deflected mode shape. This differs from the fluid pressure generated by a vibrating slender cantilever, which only depends on its local displacement at a given position. As such, the resonant frequency of a cantilevered sheet of zero aspect ratio is expected to also depend on the shape of the clamp used to restrain it. That is, a horizontally aligned cantilever that is clamped into a vertical wall will exhibit different dynamics to that of an identical cantilever held by a

a)Email: jsader@unimelb.edu.au

rigid horizontal sheet. While Atkinson and de Lara studied the rigid horizontal sheet clamp, no comparison was made with other practical clamping configurations, e.g., a vertical wall and/or a line clamp.[14,28] The principal aim of this article is to fill this gap in the literature and provide analytical formulas and numerical results for these three complementary cases. This is critical to the analysis and interpretation of measurements that naturally make use of cantilevers of low aspect ratio.[14,16,17,28,29] The flexural modes of vibration are considered throughout.

We begin by reviewing the framework of Atkinson and de Lara[27] for a 2D cantilever clamped into a horizontal sheet, which provides the theoretical foundation for this study. This previous formulation is then extended and applied to clamps in the form of a rigid line and a vertical wall. The resulting formulas for these three complementary cases are joined to the slender cantilever formula of Chu[19] using a matched asymptotic approach. This produces a formula, Eq. (33) (to be used with Eqs. (29) and (35)), that is universally valid for all aspect ratios and mode numbers. Finite element analysis is used to assess and validate the accuracy of these results. This development also allows for rigorous assessment of the empirical formulas for arbitrary aspect ratio proposed by Pabst[2] and Lindholm *et al.*[3]

II. ZERO ASPECT RATIO CANTILEVERED SHEET

We first define the overriding assumptions used in this study and briefly review the theoretical framework of Atkinson and de Lara.[27]

The cantilevered sheet consists of a thin elastic plate of rectangular platform. Its length is L, width is b, and thickness is h. One edge of the sheet that is aligned in the long axis direction is restrained in a clamp while the other three edges are free to vibrate with angular frequency, ω. The sheet thickness is infinitesimal relative to the plan view dimensions, i.e., $h/L, h/b \to 0$. The vibration amplitude of the sheet is also assumed to be infinitesimally small. As such, the sheet deformation obeys the small deflection theory of thin elastic plates.[30] The fluid is incompressible with density, ρ, and the inviscid approximation is used throughout. In this initial part of our study, we consider the limiting case of a sheet whose width greatly exceeds its length, i.e., its aspect ratio, $L/b \to 0$.

Three practically relevant clamping configurations for the cantilevered sheet are analyzed: (i) the horizontal sheet clamp, which was previously studied by Atkinson and de Lara,[27] (ii) the line clamp which approximates a cantilevered sheet held by a thin rigid pole,[14,28] and (iii) the commonly used vertical wall clamp.

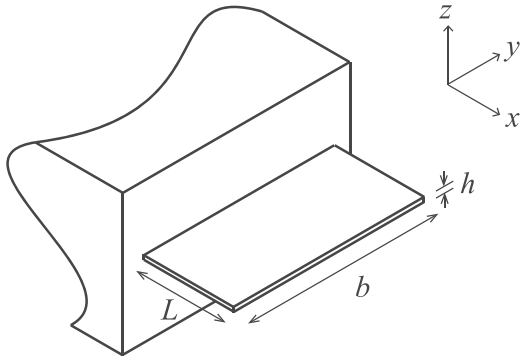

FIG. 1. Schematic illustration showing all dimensions of a rectangular cantilever and the Cartesian coordinate system. Origin of the coordinate system is at the center-of-mass of the sheet's cross section at its clamped end.

A Cartesian coordinate system is implemented such that the cantilevered sheet lies in the x-y plane with the clamp at $x = 0$ and the free end at $x = L$. The sheet is uniform and extends infinitely in the y-direction. A schematic of a cantilevered sheet clamped into a vertical wall is given in Fig. 1, showing all cantilever dimensions in perspective and the coordinate system. All clamping configurations are illustrated in Fig. 2 which also shows the fundamental mode of vibration.

A. Flow field and pressure distribution generated by a vibrating sheet

General formulas for the flow field and pressure distribution generated by a cantilevered elastic sheet immersed in fluid are now presented for the limiting case, $L/b \to 0$.[27] These formulas are then coupled to the small deflection theory of thin elastic plates[30] to examine the dynamics of these resonating structures.

Under the above-stated assumptions, a vibrating cantilever immersed in fluid generates a potential flow that satisfies the incompressible continuity condition and the linearized Bernoulli equation[31]

$$\nabla \cdot \mathbf{u} = 0, \quad p + \rho \frac{\partial \phi}{\partial t} = 0, \tag{1}$$

where p is the pressure, t is the time, and ϕ is the velocity potential and is related to the (2D) velocity field by $\mathbf{u} = \nabla\phi = \partial\phi/\partial x\,\hat{\mathbf{x}} + \partial\phi/\partial z\,\hat{\mathbf{z}}$ with $\hat{\mathbf{x}}$ and $\hat{\mathbf{z}}$ being unit vectors

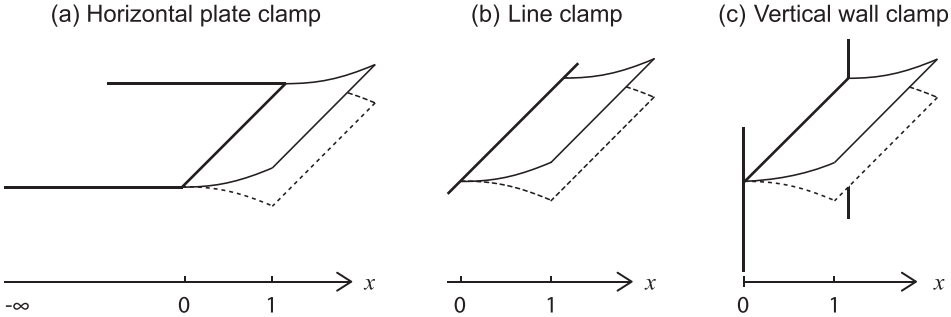

FIG. 2. Schematic diagrams of a cantilevered sheet in the small aspect ratio limit, $L/b \ll 1$, with three different clamping configurations. The fundamental mode of the resonant oscillation is illustrated (deflection magnitude not to scale). The x-axis is dimensionless.

in the x and z directions, respectively; flow in the y-direction is zero in this $L/b \to 0$ limit.

We assume an explicit time dependence of $\exp(-i\omega t)$ for the flow (and cantilever deformation) and scale all variables as follows: the spatial coordinates are scaled by the sheet's length, L; time by the reciprocal of the oscillation frequency, ω^{-1}; and the fluid velocity by $U = \omega W$, where W is the displacement amplitude at the sheet's free end. These lead to the following scales for the flow: velocity potential is scaled by LU and the fluid pressure by $\rho\,\omega LU$. All variables in Section II A (only) shall henceforth refer to their non-dimensional quantities. Equation (1) then becomes

$$\nabla^2\phi = 0, \tag{2}$$

$$p = i\phi. \tag{3}$$

Flow generated by a vibrating sheet of infinitesimal thickness is solved using a singularity method. Specifically, the Laplace equation, Eq. (2), has a point singularity solution centered at $z=0$ (the position of the sheet) and $x=s$, given by

$$\phi = \arctan\left(\frac{z}{x-s}\right). \tag{4}$$

General solution to the Laplace equation can then be constructed by linear superposition, leading to the required result

$$\phi(x,z) = \int_{-\infty}^{\infty} f(s)\arctan\left(\frac{z}{x-s}\right) ds, \tag{5}$$

where $f(s)$ is an (as yet) unspecified function to be determined by imposing the boundary conditions.

The sheet generates a flow whose pressure distribution is antisymmetric about the $z=0$ plane,[25] i.e.,

$$p|_{z=0^+} = -p|_{z=0^-}, \tag{6}$$

and the appropriate branch of the arctan function in Eq. (5) is chosen to be

$$\arctan\left(\frac{z}{x-s}\right) = \begin{cases} \pi, & z=0^+, \quad x<s \\ 0, & z=0^+, \quad x>s \\ -\pi, & z=0^-, \quad x<s \\ 0, & z=0^-, \quad x>s. \end{cases} \tag{7}$$

The no-penetration condition for inviscid flow is imposed at the sheet's surface, leading to continuity of the sheet's normal (z-component) velocity and that of the fluid at $z=0$.

While the flow will separate at the unclamped edge of the cantilevered sheet (at $x=1$) in a real viscous flow, its (nonlinear) effect on the overall dynamics will decrease with a reduction in oscillation amplitude. This is demonstrated by excellent agreement between the large aspect ratio inviscid theory of Chu[19] and measurements on macroscopic plates in Ref. 3. As mentioned above, we consider the limiting case of zero oscillation amplitude where a linear analysis is formally valid.

Next, we quote the result for the pressure jump across the cantilevered sheet derived by Atkinson and de Lara[27] for a rigid horizontal plane clamp. This is followed by new formulas for a rigid line and vertical wall clamp, the derivations of which are relegated to the Appendix for clarity. These complementary formulas are used in Section II B to calculate the resonant frequencies of the cantilever and explore the effect of varying the clamping configuration.

1. Horizontal plate clamp

Atkinson and de Lara[27] calculated the pressure distribution over a cantilevered sheet that is clamped into a rigid semi-infinite horizontal thin plate; see Fig. 2(a). The fixed edge of the cantilever lies at $x=z=0$, with the no-penetration condition for the fluid across the clamp given by $u_z=0$ for $x<0$ and $z=0^{\pm}$. The pressure jump over the sheet's vibrating upper and lower surfaces ($0 \le x \le 1$) has the closed form expression[27]

$$\Delta p = \frac{2i}{\pi}\int_0^1 v(\xi)\log\left|\frac{\sqrt{1-x}-\sqrt{1-\xi}}{\sqrt{1-x}+\sqrt{1-\xi}}\right| d\xi, \tag{8}$$

where $\Delta p \equiv p|_{z=0^+} - p|_{z=0^-}$ and $v(\xi)$ is the sheet's non-dimensional local velocity in the z-direction at position ξ. This provides an explicit expression for the pressure jump across the sheet.

2. Line clamp

The cantilevered sheet is fixed along the line $x=z=0$; see Fig. 2(b). This can be realized in practice by clamping the sheet into a thin rigid cylinder that is restrained from rotating.[14,28] This leads to the required mixed boundary conditions:

1. The fluid velocity normal to the sheet is continuous over the sheet's surface, i.e.,

$$u_z|_{z=0^+} = u_z|_{z=0^-} = v(x), \quad 0 \le x \le 1, \tag{9}$$

where u_z is the (normal) z-component of the fluid velocity.
2. Away from the cantilever, the pressure is antisymmetric about the symmetry plane $z=0$

$$\phi|_{z=0} = 0, \quad x<0 \cup x>1. \tag{10}$$

The function $f(s)$ in Eq. (5) is uniquely determined from Eqs. (9) and (10), leading to the required expression for the pressure jump for $0 \le x \le 1$

$$\Delta p = \frac{2i}{\pi}\int_0^1 v(\xi)\log\left|\frac{\sqrt{(1-x)\xi}-\sqrt{(1-\xi)x}}{\sqrt{(1-x)\xi}+\sqrt{(1-\xi)x}}\right| d\xi, \tag{11}$$

the derivation of which is presented in Appendix A 1.

3. Vertical wall clamp

Here, the elastic sheet is clamped at a 90° orientation into a rigid and unbounded vertical wall at $x=0$; see Fig. 2(c). The flow is thus restricted to the half space $x \ge 0$, with

the horizontal flow velocity $u_x = 0$ at $x = 0$. The pressure jump across the sheet in this case takes the form of a double integral

$$\Delta p = \frac{4i}{\pi}\int_0^1 v(\xi)\sqrt{\xi(1-\xi^2)}\int_x^1 \frac{s\,ds}{(\xi^2-s^2)\sqrt{1-s^2}}\,d\xi. \quad (12)$$

The reader is referred to Appendix A 2 for a derivation of this result.

B. Fluid-structure interaction of a vibrating cantilever

Next, we turn our attention to calculation of the resonant frequencies of a cantilevered sheet immersed in fluid. For a 2D flat elastic sheet, infinitely wide in the y-direction, the governing (dimensional) equation for its deflection, $w(x, t)$, in the z-direction is[30]

$$D\frac{\partial^4 w}{\partial x^4} + \rho_c h\frac{\partial^2 w}{\partial t^2} = P_{\text{fluid}}, \quad (13)$$

where $D \equiv Eh^3/(12(1-\nu^2))$ is the flexural rigidity of the sheet in which E is the Young's modulus, ν is the Poisson's ratio, ρ_c is the mass density of the sheet, and P_{fluid} is the fluid reaction net pressure (in the z-direction). The associated boundary conditions for the cantilever are

$$w(0,t) = \left.\frac{\partial w}{\partial x}\right|_{x=0} = \left.\frac{\partial^2 w}{\partial x^2}\right|_{x=L} = \left.\frac{\partial^3 w}{\partial x^3}\right|_{x=L} = 0. \quad (14)$$

Using the same scaling as in Section II A, all variables in Eqs. (13) and (14) are nondimensionalized. Specifically, the x-coordinate is scaled by L, the deflection function by W, time by ω^{-1}, and fluid reaction pressure by $\rho\omega^2 LW$. An explicit time dependence of $\exp(-i\omega t)$ is again implemented. Scaled variables are used from this point forward in Section II.

Importantly, the fluid reaction net pressure, $P_{\text{fluid}} \equiv -\Delta p$, differs for the three clamping configurations solved in Section II A, but they can all be expressed in the general form

$$P_{\text{fluid}} = -2i\int_0^1 v(\xi)g(x,\xi)\,d\xi, \quad (15)$$

where $g(x, \xi)$ is the "pressure kernel" for each clamp, specified in Eqs. (8), (11), and (12), respectively. These expressions are

$$g(x,\xi) = \frac{1}{\pi}\begin{cases} \log\left|\dfrac{\sqrt{1-x}-\sqrt{1-\xi}}{\sqrt{1-x}+\sqrt{1-\xi}}\right|, & \text{Horizontal plate clamp} \\ \log\left|\dfrac{\sqrt{(1-x)\xi}-\sqrt{(1-\xi)x}}{\sqrt{(1-x)\xi}+\sqrt{(1-\xi)x}}\right|, & \text{Line clamp} \\ \displaystyle\int_x^1 \frac{2s\sqrt{\xi(1-\xi^2)}}{(\xi^2-s^2)\sqrt{1-s^2}}\,ds, & \text{Vertical wall clamp.} \end{cases} \quad (16)$$

Equations (13)–(15) then give the required (dimensionless) governing equation for a cantilever vibrating in fluid

$$\frac{d^4 w}{dx^4} - \Omega^2\left(w - 2\Lambda\int_0^1 w(\xi)g(x,\xi)\,d\xi\right) = 0, \quad (17)$$

with boundary conditions,

$$w(0) = w'(0) = w''(1) = w'''(1) = 0. \quad (18)$$

The scaled resonant frequency, Ω, is defined

$$\Omega = \omega\sqrt{\frac{\rho_c h L^4}{D}}, \quad (19)$$

and the added mass parameter is

$$\Lambda = \frac{\rho L}{\rho_c h}. \quad (20)$$

Note that the resonant frequency, Ω, in fluid for a given clamping configuration is completely characterized by the added mass parameter, Λ. It is the ratio of oscillatory fluid inertia to inertia in the solid structure. It, therefore, provides a measure of the relative strength of fluid loading on the cantilevered sheet.

C. Resonant frequencies in fluid

Equation (17) and its associated boundary conditions in Eq. (18) are solved using a (spectral) Galerkin method. The basis functions are chosen to satisfy Eq. (18) whose governing equation is that for a flat elastic sheet in vacuum

$$\frac{d^4\Phi_k}{dx^4} - C_k^4\Phi_k = 0, \quad (21)$$

where

$$\Phi_k(0) = \Phi_k'(0) = \Phi_k''(1) = \Phi_k'''(1) = 0, \quad (22)$$

and the eigenvalue, C_k, is the k-th positive root of

$$1 + \cos C_k \cosh C_k = 0, \quad (23)$$

with $k = 1, 2, 3,\ldots$. Solutions to Eqs. (21) and (22) form a complete orthonormal basis set; explicit expression for Φ_k can be found in Eq. (24) of Ref. 18. The required deflection function, w, of the cantilever immersed in fluid is specified by a general linear combination of the basis modes, Φ_k. This infinite series is truncated at N terms

$$w(x) = \sum_{k=1}^{N} a_k \Phi_k(x), \tag{24}$$

and the number of terms systematically increased until convergence is achieved; the coefficients, a_k, are determined in the process (see below).

Substituting Eq. (24) into Eq. (17), and making use of Eq. (21), then gives

$$\sum_{k=1}^{N} a_k \left[(C_k^4 - \Omega^2)\Phi_k(x) + 2\Omega^2 \Lambda \int_0^1 \Phi_k(\xi) g(x,\xi)\, d\xi \right] = 0. \tag{25}$$

Using orthogonality of Φ_m leads to the following linear system of equations for the unknown coefficients, a_k, and the resonant frequency, Ω,

$$\sum_{k=1}^{N} \left[\left(C_m^4 - \Omega^2\right)\delta_{mk} + \Omega^2 \Lambda T_{mk} \right] a_k = 0, \tag{26}$$

where $m = 1, 2, 3,\ldots, N$, and

$$T_{mk} = 2 \int_0^1 \int_0^1 \Phi_m(x)\Phi_k(\xi) g(x,\xi)\, dx\, d\xi, \tag{27}$$

and δ_{mk} is the Kronecker delta function.

Thus, for a specified added mass parameter, Λ, the resonant frequencies, Ω, of the cantilever are determined by solving the eigenvalue equation

$$\det\left[\left(C_m^4 - \Omega^2\right)\delta_{mk} + \Omega^2 \Lambda T_{mk} \right] = 0. \tag{28}$$

The coefficients, a_k, are then evaluated from Eq. (26), which immediately gives the modes shapes via Eq. (24).

Mode n of the cantilevered sheet is specified by the n-th root of Eq. (28), yielding the normalized frequency, Ω_n, where $n = 1, 2, 3,\ldots, N$.

III. ARBITRARY ASPECT RATIO

The effect of fluid loading on the resonant frequencies of a thin cantilevered sheet, in the large aspect ratio limit, is often characterized by its hydrodynamic function, Γ,[18] i.e.,

$$\omega_{\text{fluid}} = \omega_{\text{vac}} \left(1 + \frac{\pi \rho b}{4 \rho_c h} \Gamma \right)^{-1/2}, \tag{29}$$

where the subscripts "fluid" and "vac" refer to the resonant frequencies in fluid and vacuum, respectively. In this large aspect ratio limit[19,24,25]

$$\Gamma_{\text{large}} = 1, \quad \frac{L}{b} \gg 1, \tag{30}$$

for small mode numbers, $n \ll L/b$. In the opposite limit of small aspect ratio, Eq. (17) gives

$$\Gamma_{\text{small}} = \frac{4L}{\pi b} \alpha_{\text{small}}, \quad \frac{L}{b} \ll 1, \tag{31}$$

where α_{small} is henceforth termed the "rescaled hydrodynamic function" and is an order one coefficient that depends on the specific clamping configuration used, mode number, n, and the hydrodynamic loading via the added mass parameter, Λ.

In the asymptotic limit of large n[24,25]

$$\Gamma = \frac{8}{n\pi^2} \frac{L}{b}, \quad \left(n \gg \frac{L}{b} \right) \text{ and } (n \gg 1), \tag{32}$$

regardless of the cantilever's aspect ratio, L/b.

A composite solution can then be constructed from the asymptotic results in Eqs. (30)–(32) using a Padé approximant, giving the required result

$$\Gamma = \left(1 + \frac{\pi}{4\alpha_{\text{small}}} \frac{b}{L} \right)^{-1}. \tag{33}$$

This simple formula holds for all aspect ratios, L/b, and all mode numbers, n.

Analogous to Eq. (31), the hydrodynamic function for all aspect ratios can be rescaled to give

$$\alpha \equiv \frac{\pi b}{4L} \Gamma. \tag{34}$$

This expression is used in the examination of the accuracy of Eq. (33) in Section IV B.

IV. NUMERICAL RESULTS

In this section, we first present numerical results for the resonant frequencies of a cantilevered sheet of zero aspect ratio, i.e., $L/b \to 0$, and examine the effect of clamping configuration. The dependence on mode number is also studied. This is achieved using the theoretical formulation in Section II C. This is followed by a comparison of Eq. (33) with rigorous finite element solutions of a cantilevered sheet with finite aspect ratio.

A. Zero aspect ratio

The theory in Section II C is implemented in MATHEMATICA®10.0. The number of basis modes, N, in Eq. (24) are systematically increased to achieve a convergence greater than 99.9% in the rescaled hydrodynamic function, α_{small}, for the first 10 modes; $N = 12$ gives this required precision. The number of basis modes needed, N, increases with mode number, n, and fluid strength, Λ. This suggests that the mode shapes in fluid may also change as a result of increasing fluid loading; this is studied below.

1. Effect of clamping configuration

The (dimensionless) hydrodynamic function, Γ, specifies the effect of the surrounding fluid on the resonant

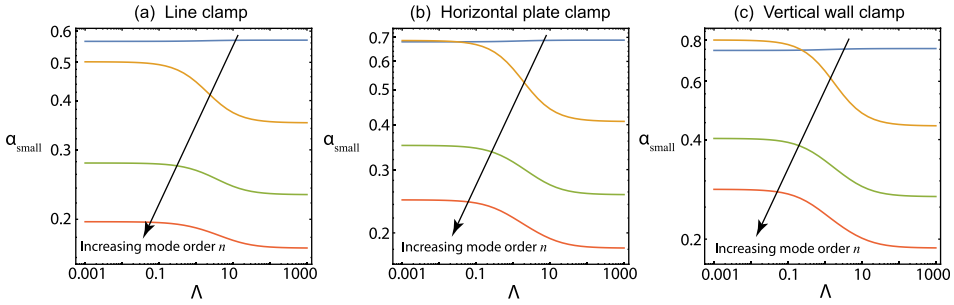

FIG. 3. Rescaled hydrodynamic functions, α_{small}, for the first four resonant modes ($n = 1, 2, 3, 4$) as a function of the added mass parameter, Λ. (a), (b), and (c) give results for the line clamp, horizontal plate clamp, and vertical wall clamp, respectively.

frequencies of the cantilever; see Eq. (29). For a sheet of zero aspect ratio, under consideration in this section, it is more natural to use the rescaled hydrodynamic function, α_{small}, as defined in Eq. (31). Numerically, this parameter is calculated using $\alpha_{small} = (C_n^4/\Omega^2 - 1)/\Lambda$.

Figure 3 gives the rescaled hydrodynamic function, α_{small}, as a function of the clamping configuration and the added mass parameter, Λ. The function, α_{small}, is clearly delineated into two separate regions, with a transition occurring at $\Lambda \sim \mathcal{O}(1)$. This coincides with the added mass of the fluid (due to its inertia) being comparable with the actual mass of the cantilevered sheet. In such cases, the fluid loading is strong and thus can potentially impact the mode shapes of vibration.

The results in Fig. 3 establish that changing the clamp from one that is a horizontal sheet to a line clamp and finally to a vertical wall strongly affects the resonant frequencies of all modes. This is expected because the 2D potential flow generated by a vibrating zero aspect ratio cantilever always exhibits nonlocal behaviour, i.e., the pressure at any position depends on the overall mode shape rather than the deflection at that point.

To highlight this behavior, Fig. 4 shows a direct comparison of α_{small} for these three clamping configurations. The line clamp is observed to exhibit the smallest value of α_{small}, as may be expected because it provides the least obstruction to the flow. The horizontal plate possesses the next largest value of α_{small}, followed by the vertical wall clamp. These results provide guidance for the design of clamps of cantilevered sheets, in cases where the effect of the surrounding fluid is to be minimized or maximized.

Interestingly, the rescaled hydrodynamic function for the fundamental mode ($n = 1$) is very weakly dependent on the added mass parameter, Λ. This function increases only slightly as Λ is varied from zero to infinity. In contrast, the higher order modes ($n > 1$) display a much stronger effect, but now decrease with increasing Λ; see Figs. 3 and 4.

The results in Fig. 4 also show that the clamp affects the fundamental mode frequency weakly, relative to modes 2, 3, and 4. Taken collectively, these observations suggest that the deflection functions, w, of the higher order modes are more strongly affected than those of the fundamental mode ($n = 1$). The physical mechanisms giving rise to these features are examined in Section IV A 2.

2. Mode shapes and pressure distributions

Figure 5 gives the deflection functions (mode shapes) and pressure distributions for the first 3 modes of a cantilevered sheet with a line clamp, as a function of the added mass parameter, Λ; analogous results for horizontal plate and vertical wall clamps are presented in Section S1 of the supplementary material.

The deflection function, w, for the fundamental mode ($n = 1$) is weakly dependent on the strength of fluid loading; see Fig. 5(a). This observation is consistent with the results for the pressure distribution in Fig. 5(d), which also show very little variation with respect to Λ. This explains why the rescaled hydrodynamic function, α_{small}, for the fundamental mode varies only slightly with the fluid loading strength; see Fig. 4.

The behavior of modes 2 and 3, however, is markedly different with the deflection function and pressure distribution varying strongly with Λ; see Figs. 5(b), 5(c), 5(e), and 5(f). While the fundamental mode exhibits a very simple deflection function, increasing monotonically with distance from the clamp, the higher order modes contain nodes, i.e., where the displacement is zero. This facilitates an adjustment in the hydrodynamic pressure through a change in the positions of these nodes, when the fluid loading is strong. The dramatically different mode shapes, relative to light fluid loading, then leads to a strong change in the rescaled hydrodynamic function, α_{small}, for $\Lambda \gtrsim \mathcal{O}(1)$.

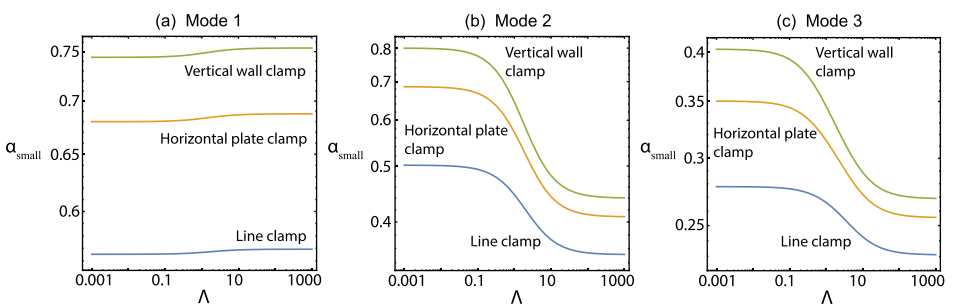

FIG. 4. Comparison of the rescaled hydrodynamic function, α_{small}, for different clamping configurations. Results given for the first three resonant modes in (a), (b), and (c).

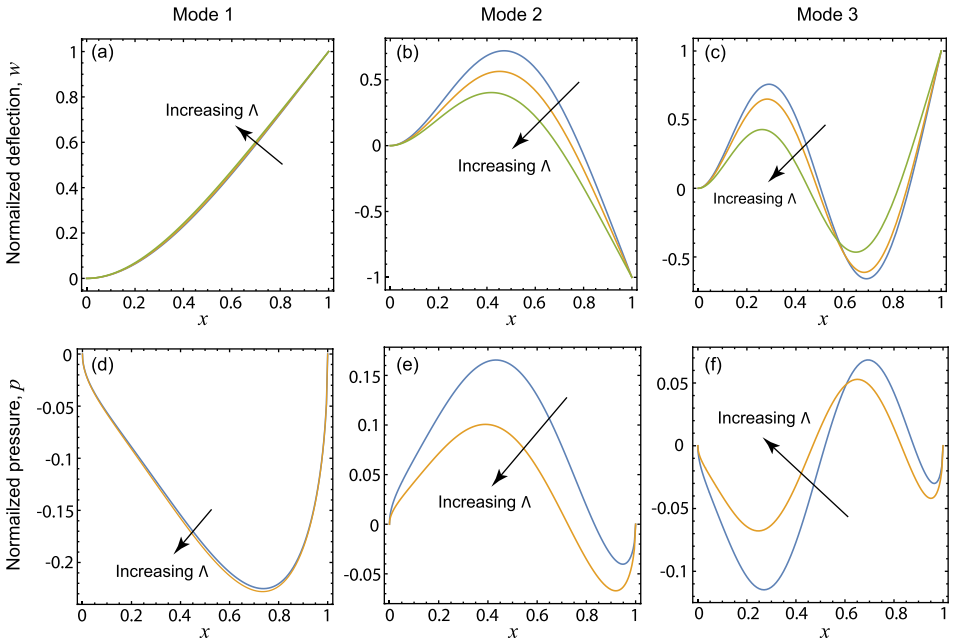

FIG. 5. Normalized deflection functions and pressure distributions for a cantilevered sheet with a line clamp, for the first three modes. In (a), (b), and (c), deflection functions are given for increasing added mass parameter, $\Lambda = 0$, 1, and 100, corresponding to vacuum, light, and heavy fluid load conditions, respectively. In (d), (e), and (f), pressure distributions are compared for moderate and heavy fluid loads, specifically when $\Lambda = 1$ and $\Lambda = 100$, respectively.

3. Limit of high mode number

Despite the above-mentioned variations in the rescaled hydrodynamic function for modes 2 and 3, Eq. (32) indicates that the resonant frequency is insensitive to the clamping configuration in the limit of high mode number, i.e., $n \gg 1$. This suggests that the influence of the clamp diminishes with increasing n, with the exception of the singular case, $n = 1$.

Numerical results for the line clamp are given in Fig. 6, which provides a comparison of the predictions of Eq. (32) with numerical results in the limits of small and large Λ. The large n asymptotic solution lies between the small and large Λ results. As the mode number, n, increases, these upper and lower values approach the large n solution; note that a logarithmic vertical scale is used to highlight the relative differences. This verifies the above prediction that the fluid's effect on the rescaled hydrodynamic function diminishes with increasing n. While the flow is strictly nonlocal, as discussed in Section IV A 1, increasing mode number restricts the domain in x over which this nonlocality applies. In the asymptotic limit of large n, the deflection functions are sinusoidal with small wavelength relative to the cantilever length, L. This ensures a strict local dependence of the pressure distribution on position, x.

The horizontal plate and vertical wall clamps also display convergence of the high and low Λ solutions, but this occurs for larger n; see Section S2 of the supplementary material.

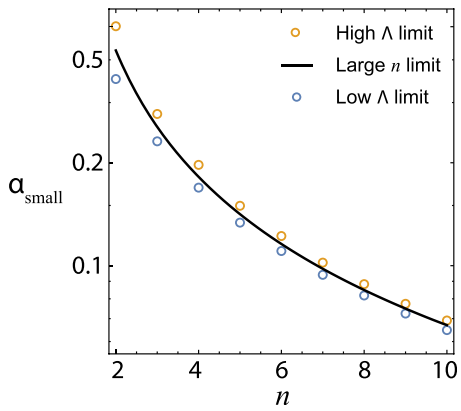

FIG. 6. Rescaled hydrodynamic function, α_{small}, for a cantilevered sheet with a line clamp as a function of mode number, n. The range that α_{small} varies in response to increasing fluid load, Λ, is indicated by the vertical distance between the two open circles for each n. The large mode number asymptotic result is the solid curve. A logarithmic scale is used for the vertical axis to facilitate comparison.

4. Empirical fit function

To facilitate application in practice, the generated numerical results for the rescaled hydrodynamic function are fitted to the following empirical equation:

$$\alpha_{\text{small}} = \frac{\alpha_{\text{small}}^{(0)} + \alpha_{\text{small}}^{(\infty)} \Lambda^c}{1 + \Lambda^c}, \tag{35}$$

where the parameters $\alpha_{\text{small}}^{(0)}$ and $\alpha_{\text{small}}^{(\infty)}$ are the values of α_{small} in the limits of small and large added mass parameter, Λ, whereas c is determined using a nonlinear least squares fit for each mode number and clamping configuration. Numerical values for these parameters are listed in Table I. The error of the resulting fit function, Eq. (35), relative to the calculated numerical results using the theory in Section II, is also provided.

B. Arbitrary aspect ratio

Equation (33) together with Eqs. (29) and (35) allow the resonant frequencies of a cantilevered sheet of arbitrary aspect ratio, L/b, to be calculated. Importantly, Eq. (33) is derived by linking the results for small and large aspect ratio using a matched asymptotic approach. It is therefore important to examine and validate its accuracy. This is performed here by comparing its prediction with rigorous finite element

TABLE I. Fit parameters for Eq. (35) and the maximum relative error this formula exhibits for all Λ. Results given as a function of clamping configuration and mode number, n.

Mode number, n	$\alpha_{\text{small}}^{(0)}$	$\alpha_{\text{small}}^{(\infty)}$	c	Error (%)
Horizontal plate clamp				
1	0.680	0.687	0.974	0.1
2	0.693	0.415	0.981	3.2
3	0.355	0.259	0.847	2.6
4	0.250	0.183	0.833	1.8
5	0.182	0.143	0.781	1.9
6	0.148	0.117	0.776	1.5
7	0.120	0.0986	0.739	1.6
8	0.104	0.0852	0.737	1.4
9	0.0890	0.0752	0.706	1.4
10	0.0795	0.0669	0.698	1.3
Line clamp				
1	0.565	0.569	0.939	0.1
2	0.507	0.357	0.949	3.1
3	0.282	0.234	0.756	3.0
4	0.200	0.171	0.698	2.5
5	0.152	0.135	0.605	2.2
6	0.124	0.111	0.573	1.9
7	0.104	0.0947	0.508	1.7
8	0.0895	0.0823	0.488	1.6
9	0.0785	0.0728	0.435	1.4
10	0.0702	0.0651	0.412	1.4
Vertical wall clamp				
1	0.744	0.754	0.986	0.1
2	0.807	0.447	0.994	2.8
3	0.407	0.272	0.872	1.9
4	0.285	0.189	0.861	0.9
5	0.204	0.146	0.823	1.1
6	0.165	0.119	0.818	0.8
7	0.133	0.100	0.792	1.0
8	0.114	0.0863	0.789	0.8
9	0.0975	0.0761	0.769	0.9
10	0.0869	0.0676	0.760	0.8

solutions of the complete fluid-structure problem for a cantilever of finite aspect ratio immersed in fluid.

The finite element solution is performed with the commercial finite element software COMSOL Multiphysics, using its eigenfrequency solver. Rather than implementing the thin plate equation,[30] the cantilevered sheet is modeled using full three-dimensional solid elements. The surrounding fluid is characterized by Eq. (1), which is expressed in terms of the 3D velocity potential. At the interface between the fluid and solid domains, the usual conditions of continuity of stress, and no-penetration are imposed. This provides direct coupling between Eq. (1) and Navier's equation for the solid. The cantilever's thickness is systemically reduced to mimic the infinitesimal thickness of the theoretical model presented in Section II. A thickness-to-length ratio of 0.01 is used throughout; see Section S3 of the supplementary material which shows that finite thickness leads to an overestimation of the hydrodynamic function.[24,32] Far from the cantilever, a zero fluid pressure condition is imposed. Only the vertical wall clamp is studied here, because its impact on the cantilever's resonant frequency is greatest relative to the other clamps studied. A Poisson's ratio of 0.25 is used throughout. Systematic mesh refinement is employed. The reported results are independent of mesh and domain size, and are converged to better than 99.9%.

Figure 7 presents a comparison of results for the rescaled hydrodynamic function, α [see Eq. (34)], obtained using finite element analysis and Eq. (33). The added mass parameter, Λ [Eq. (20)], is varied to encompass fluid loading strengths ranging from small to large. Also shown in Fig. 7 are the predictions of the previous solution of Lindholm[3]

$$\Gamma_{\text{Lindholm}} = \left(1 + \frac{b}{2L}\right)^{-1}, \tag{36}$$

which is derived for all aspect ratios, L/b, by extending the empirical formula of Pabst[2]

$$\Gamma_{\text{Pabst}} = 1 - \frac{b}{2L}, \quad \frac{L}{b} > 1. \tag{37}$$

The Pabst expression is formulated for aspect ratios, L/b, greater than one only.

Importantly, the formulas of both Pabst and Lindholm do not include any dependency on the clamping configuration, mode number, or added mass parameter. This contrasts to the present formula, Eq. (33), which is derived for all aspect ratios and contains these dependencies.

The finite element results in Fig. 7 clearly demonstrate the effect of the added mass parameter and mode number on the rescaled hydrodynamic function. For mode 1, Eq. (33) accurately captures the benchmark finite element solutions for all added mass parameter values studied—here, the hydrodynamic function is very weakly dependent on the added mass parameter; see Fig. 7(a). While the Lindholm formula, Eq. (36), works well in the high aspect ratio limit (where it is formally exact), strong deviations relative to the finite element solutions emerge as aspect ratio is reduced. For small aspect ratios, the Lindholm formula strongly overestimates the hydrodynamic function (by a factor of ≈2).

Figure 7(b) shows corresponding results for mode 2, where the present solution, Eq. (33), accurately captures the

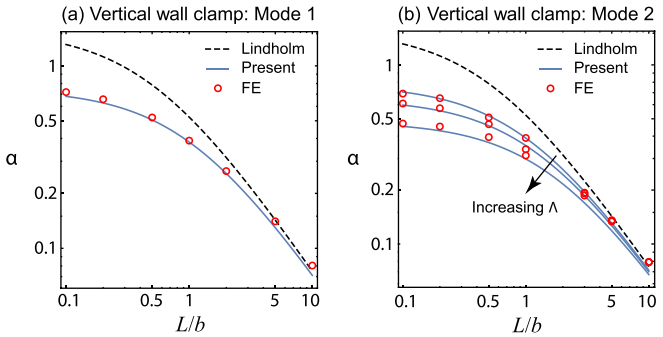

FIG. 7. Rescaled hydrodynamic function, α, for the first two modes of a cantilevered sheet with a vertical wall clamp, as a function of the sheet's aspect ratio. Solid lines are due to Eq. (33) and open circles are the finite element simulation results; dashed line is Lindholm's empirical formula, Eq. (36), which depends only on the aspect ratio. In (b) the fluid loading strength is given for Λ = 0.1, 1, and 10, while in (a) only the results of Λ = 0.1 are shown because varying Λ results in an indiscernible difference to the data shown.

dependence of α on the added mass parameter, Λ; this dependency is no longer negligible, as it was for $n=1$. The Lindholm formula does not predict any dependence on the added mass parameter, in stark disagreement with the finite element results.

The Pabst formula, Eq. (37), exhibits similar behavior to that of Lindholm (data not shown). This is entirely expected because the latter is derived from the Pabst formula. We refrain from presenting results for different clamping configurations because their behavior is comparable with those given in Fig. 7 for the vertical wall clamp.

V. CONCLUSIONS

We have investigated the effect of fluid loading on the flexural resonant frequencies of cantilevered sheets of arbitrary aspect ratio.

This was achieved by first using the formulation of Atkinson and de Lara[27] to study the effect of clamping configuration on a (2D) infinitely wide cantilever sheet, i.e., the zero aspect ratio limit. A strong dependence on clamping configuration, added mass parameter, and mode number was observed. A formula, Eq. (35), obtained by fitting the numerical results, was presented for the rescaled hydrodynamic function to facilitate application in practice.

The (2D) zero aspect ratio result was connected to the well known solution of Chu[19] for a cantilever of infinite aspect ratio, using a match asymptotic approach. A simple and universally valid formula resulted, Eq. (33) (to be used with Eqs. (29) and (35)), which exhibits excellent agreement with finite element analysis of cantilever sheets over all aspect ratios. This analysis shows that previous formulas for finite aspect ratio sheets can exhibit significant errors and do not capture the required dependence on clamping configuration, fluid loading strength, and mode number.

These results are expected to be of practical value in engineering and device design, where cantilever structures are frequently encountered.

SUPPLEMENTARY MATERIAL

See supplementary material for numerical results for horizontal plate and vertical wall clamps that are analogous to Figs. 5 and 6, and the effect of finite thickness.

ACKNOWLEDGMENTS

The authors gratefully acknowledge the support of the Australian Research Council Grants Scheme.

APPENDIX: DERIVATION OF PRESSURE DISTRIBUTION

In this Appendix, we calculate the pressure distribution on a vibrating cantilever of zero aspect ratio immersed in fluid, for two distinct clamping configurations: (1) a line clamp and (2) a vertical wall. This is achieved by determining the unknown function, $f(s)$, in Eq. (5) for each clamping configuration.

1. Line clamp

The boundary conditions for the flow field are given in Eqs. (9) and (10). Using the principal branch in Eq. (7), the velocity potential, ϕ, in Eq. (5) at the cantilever surface ($z=0$) is

$$\phi|_{z=0^{\pm}} = \pm\pi \int_x^{\infty} f(s)\, ds. \tag{A1}$$

The zero pressure condition away from the cantilever, Eq. (10), is then enforced giving

$$f(s) = 0, \quad s < 0 \cup s > 1, \tag{A2}$$

and

$$\int_0^1 f(s)\, ds = 0. \tag{A3}$$

Differentiating Eq. (5) with respect to z gives the fluid velocity in the z-direction

$$\frac{\partial \phi}{\partial z} = \int_0^1 \frac{f(s)}{(x-s)\left[1+\left(\frac{z}{x-s}\right)^2\right]}\, ds, \tag{A4}$$

which can be evaluated at $z=0$ to give an integral equation relating $f(s)$ to the normal velocity of the cantilever

$$v(x) = \int_0^1 \frac{f(s)}{x-s}\, ds, \quad 0 \le x \le 1, \tag{A5}$$

where the singular integral is defined as a Cauchy principal value. The general solution to this integral equation is[33]

$$f(s) = \frac{1}{\pi^2\sqrt{s(1-s)}} \int_0^1 v(\xi) \frac{\sqrt{\xi(1-\xi)}}{\xi - s}\, d\xi + \frac{C}{\sqrt{s(1-s)}}, \tag{A6}$$

where the constant $C=0$ is specified by Eq. (A3).

Equations (A1) and (3) then give the required pressure jump along the cantilever's surface

$$\Delta p = \frac{2i}{\pi} \int_0^1 v(\xi) \log \left| \frac{\sqrt{(1-x)\xi} - \sqrt{(1-\xi)x}}{\sqrt{(1-x)\xi} + \sqrt{(1-\xi)x}} \right| d\xi. \tag{A7}$$

2. Vertical wall

To calculate the pressure distribution for a cantilevered sheet clamped into a vertical wall, we reflect the cantilever along the negative x-axis and remove the wall. This produces an identical flow to the original problem with the origin at the original clamp position.

The required boundary conditions for this equivalent flow are specified on the entire line $z=0$, which yields even solutions (with respect to x) for the velocity field and pressure

$$v(x) = u_z(x) = u_z(-x), \quad -1 \le x \le 1, \tag{A8}$$

$$\Delta p = 0, \quad |x| > 1. \tag{A9}$$

The function $f(s)$ to be solved is subject to

$$f(s) = 0, \quad |s| > 1, \tag{A10}$$

and

$$\int_{-1}^{1} f(s)\, ds = 0. \tag{A11}$$

Equations (A8) and (5) give the required integral equation for $f(s)$

$$v(x) = \int_{-1}^{1} \frac{f(s)}{x - s}\, ds, \quad -1 \le x \le 1, \tag{A12}$$

whose general solution is[33]

$$f(s) = \frac{A}{\sqrt{1 - s^2}} + \frac{2s}{\pi^2 \sqrt{1 - s^2}} \int_0^1 \frac{v(\xi)\sqrt{1 - \xi^2}}{\xi^2 - s^2}\, d\xi, \tag{A13}$$

where the constant $A = 0$ is determined from Eq. (A11).

This analysis gives the required pressure jump over $0 \le x \le 1$, for the original cantilever problem

$$\Delta p = \frac{4i}{\pi} \int_0^1 v(\xi) \sqrt{\xi(1 - \xi^2)} \int_x^1 \frac{s\, ds}{(\xi^2 - s^2)\sqrt{1 - s^2}}\, d\xi. \tag{A14}$$

[1]R. Berger, C. Gerber, H. P. Lang, and J. K. Gimzewski, Microelectron. Eng. **35**, 373 (1997).
[2]W. Pabst, N.A.C.A. Technical Memorandum 580, 1930.
[3]U. S. Lindholm, D. D. Kana, W.-H. Chu, and H. N. Abramson, J. Ship Res. **9**, 11 (1965).
[4]L. Landweber, J. Ship Res. **11**, 143 (1967).
[5]G. Binnig, C. F. Quate, and C. Gerber, Phys. Rev. Lett. **56**, 930 (1986).
[6]J. E. Sader, J. W. M. Chon, and P. Mulvaney, Rev. Sci. Instrum. **70**, 3967 (1999).
[7]C. P. Green and J. E. Sader, J. Appl. Phys. **98**, 114913 (2005).
[8]T. Fukuma, Rev. Sci. Instrum. **80**, 023707 (2009).
[9]C. A. Van Eysden and J. E. Sader, J. Appl. Phys. **101**, 044908 (2007).
[10]J. E. Sader, T. P. Burg, and S. R. Manalis, J. Fluid Mech. **650**, 215 (2010).
[11]L. Tang, M. P. Paidoussis, and J. Jiang, J. Sound Vib. **326**, 263 (2009).
[12]J. A. Dunnmon, S. C. Stanton, B. P. Mann, and E. H. Dowell, J. Fluids Struct. **27**, 1182 (2011).
[13]D. T. Akcabay and Y. L. Young, Phys. Fluids **24**, 054106 (2012).
[14]D. Kim, J. Cossé, C. Huertas Cerdeira, and M. Gharib, J. Fluid Mech. **736**, R1 (2013).
[15]S. Michelin and O. Doare, J. Fluid Mech. **714**, 489 (2013).
[16]P. S. Gurugubelli and R. K. Jaiman, J. Fluid Mech. **781**, 657 (2015).
[17]J. Ryu, S. G. Park, B. Kim, and H. J. Sung, J. Fluids Struct. **57**, 159 (2015).
[18]J. E. Sader, J. Appl. Phys. **84**, 64 (1998).
[19]W.-H. Chu, Technical Report No. 2, DTMB, Contract NObs-86396(X), Southwest Research Institute, San Antonio, Texas, 1963.
[20]G. Muthuveerappan, N. Ganesan, and M. A. Veluswami, J. Sound Vib. **61**, 467 (1978).
[21]D. G. Crighton, J. Sound Vib. **87**, 429 (1983).
[22]G. Muthuveerappan, N. Ganesan, and M. A. Veluswami, Comput. Struct. **21**, 479 (1985).
[23]Y. Fu and W. G. Price, J. Sound Vib. **118**, 495 (1987).
[24]F. J. Elmer and M. Dreier, J. Appl. Phys. **81**, 7709 (1997).
[25]C. A. Van Eysden and J. E. Sader, J. Appl. Phys. **100**, 114916 (2006).
[26]C. A. Van Eysden and J. E. Sader, J. Appl. Phys. **106**, 094904 (2009).
[27]C. Atkinson and M. M. de Lara, J. Sound Vib. **300**, 352 (2007).
[28]J. E. Sader, J. Cossé, D. Kim, B. Fan, and M. Gharib, J. Fluid Mech. **793**, 524 (2016).
[29]A. Gilmanov, T. B. Le, and F. Sotiropoulos, J. Comput. Phys. **300**, 814 (2015).
[30]S. P. Timoshenko and S. Woinowsky-Krieger, *Theory of Plates and Shells* (McGraw-Hill, 1959).
[31]G. K. Batchelor, *An Introduction to Fluid Dynamics* (Cambridge University Press, 2000).
[32]D. R. Brumley, M. Willcox, and J. E. Sader, Phys. Fluids **22**, 052001 (2010).
[33]N. Muskbelishvili, *Singular Integral Equations* (Erven P. Noordhoff, 1953).